CellPress
PARTNER JOURNAL

Molecular Plant
Research Article

A Single-Cell RNA Sequencing Profiles the Developmental Landscape of *Arabidopsis* Root

Tian-Qi Zhang[1,4], Zhou-Geng Xu[1,2,4], Guan-Dong Shang[1,2] and Jia-Wei Wang[1,2,3,*]

[1]National Key Laboratory of Plant Molecular Genetics (NKLPMG), CAS Center for Excellence in Molecular Plant Sciences, Institute of Plant Physiology and Ecology (SIPPE), Shanghai 200032, P. R. China

[2]University of Chinese Academy of Sciences, Shanghai 200032, P. R. China

[3]ShanghaiTech University, Shanghai 200031, P. R. China

[4]These authors contributed equally to this article.

***Correspondence: Jia-Wei Wang (jwwang@sippe.ac.cn)**

https://doi.org/10.1016/j.molp.2019.04.004

ABSTRACT

Cells of eukaryotic multicellular organisms have inherent heterogeneity. Recent advances in single-cell gene expression studies enable us to explore transcriptional regulation in dynamic development processes and highly heterogeneous cell populations. In this study, using a high-throughput single-cell RNA-sequencing assay, we found that the cells in *Arabidopsis* root are highly heterogeneous in their transcriptomes. A total of 24 putative cell clusters and the cluster-specific marker genes were identified. The spatial distribution and temporal ordering of the individual cells at different developmental stages illustrate their hierarchical structures and enable the reconstruction of continuous differentiation trajectory of root development. Moreover, we found that each root cell cluster exhibits distinct patterns of ion assimilation and hormonal responses. Collectively, our study reveals a high degree of heterogeneity of root cells and identifies the expression signatures of intermediate states during root cell differentiation at single-cell resolution. We also established a web server (http://wanglab.sippe.ac.cn/rootatlas/) to facilitate the use of the datasets generated in this study.

Key words: *Arabidopsis*, root, scRNA-seq, cell atlas, differentiation trajectory, meristem

Zhang T.-Q., Xu Z.-G., Shang G.-D., and Wang J.-W. (2019). A Single-Cell RNA Sequencing Profiles the Developmental Landscape of *Arabidopsis* Root. Mol. Plant. **12**, 648–660.

INTRODUCTION

Root exhibits a continuous and iterative growth habit because of the existence of stem cells (a subpopulation of meristematic cells) at its apical regions (Sharma et al., 2003). As in animals, plant stem cells can differentiate into other types of cells and also divide in the self-renewal manner. Root apical meristem (RAM) resides in the root tip (Aichinger et al., 2012; Petricka et al., 2012). The core of RAM is the stem cell niche (SCN) (Figure 1D) (Benfey, 2016), which harbors the organizing center, also known as the quiescent center (QC), and surrounding stem cells (Aichinger et al., 2012). The function of RAM is to maintain its pluripotent property and generate diverse root cell types including epidermis, hair cell, root cap, cortex, endodermis, and stele (consisting of the pericycle, phloem, xylem, and procambium) through cell division, expansion, and differentiation (Birnbaum et al., 2003; Miyashima et al., 2011; Benfey, 2016; Drapek et al., 2017). As such, the maturity of the major cell types is gradually increased along the longitudinal axis of the root in the shootward direction.

The molecular basis of root development has been extensively studied in *Arabidopsis thaliana*. It has been shown that plant hormones and transcription factors play critical role in RAM maintenance and cell differentiation. For instance, an intersection of high auxin concentration together with endodermal transcription factors controls the localization of the QC (Sabatini et al., 1999, 2003). The transcription factor WUSCHEL-RELATED HOMEOBOX 5 (WOX5), whose transcripts are exclusively detected in QC, maintains columella stem cell pluripotency by repressing the expression of *CYCLING DOF FACTOR 4* (*CDF4*), which encodes a differentiation factor (Pi et al., 2015). Accordingly, disruption of *WOX5* leads to terminal differentiation of surrounding stem cells (Sarkar et al., 2007). The transition from cell division to cell expansion and differentiation in distinct root developmental zones is guided by another group of transcription factors named PLETHORA (PLT). PLT proteins form a gradient by mitotic distribution and short distance

Published by the Molecular Plant Shanghai Editorial Office in association with Cell Press, an imprint of Elsevier Inc., on behalf of CSPB and IPPE, SIBS, CAS.

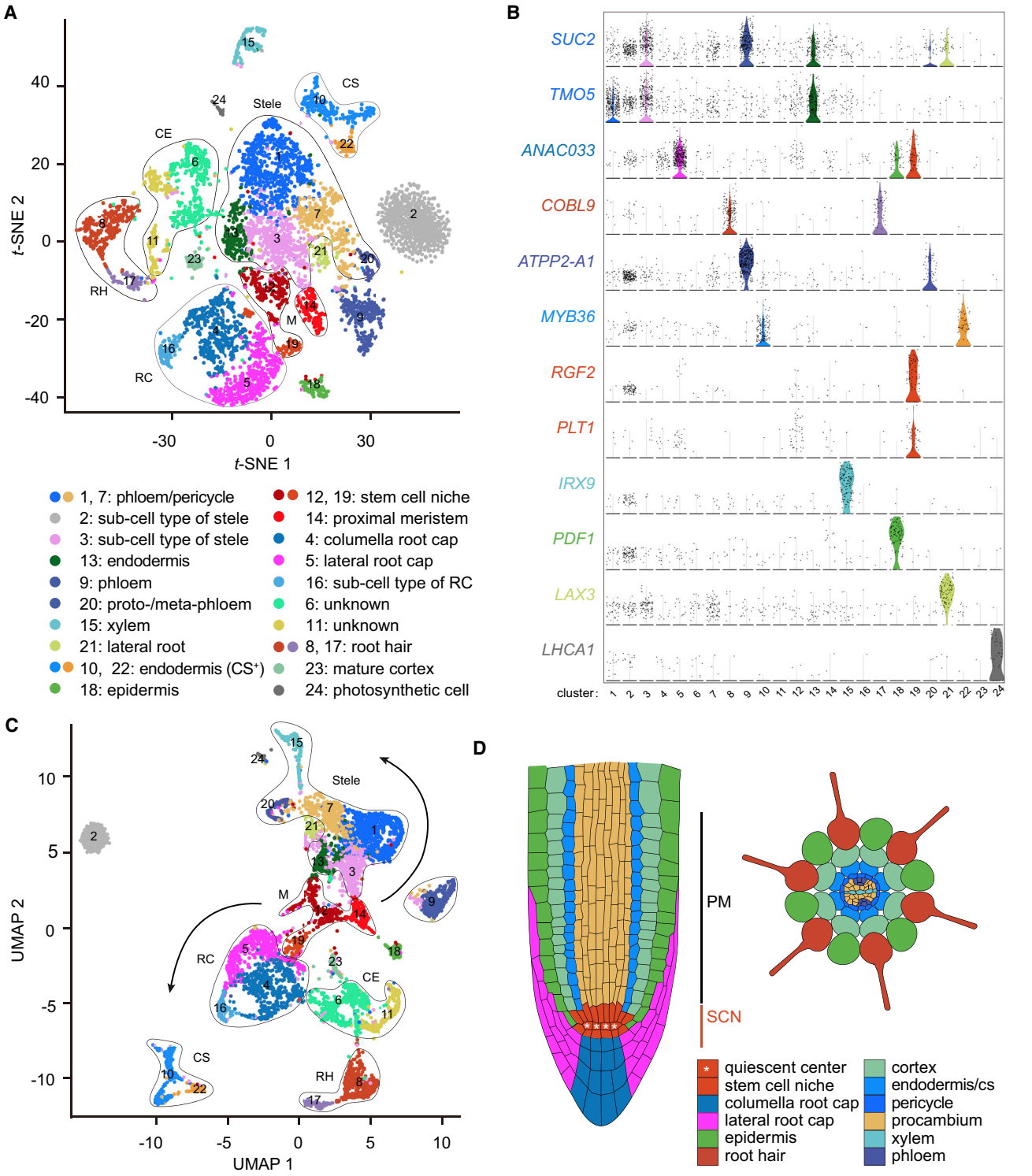

Figure 1. Cell Heterogeneity in *Arabidopsis* Root.

(A) *t*-SNE visualization to identify putative 24 cell clusters from 7695 cells in roots. Each dot denotes a single cell. Colors denote corresponding cell clusters. Clusters 1, 3, 7, and 13 represent stele without xylem and phloem. Black line surrounds a cell type. RC, root cap; CE, cell elongation; RH, root hair; CS, endodermal cells with casparian strip; PM, proximal meristem; M, meristem (SCN and PM).

(B) Violin plot showing the expression pattern of representative cell-type marker genes in 24 cell clusters. Each dot denotes a single cell.

(C) Visualization of the root cell clusters by UMAP algorithm. Two putative differentiation trajectories of stem cell niche (SCN) are shown by black curved arrows. Black outline surrounds a cell type. RC, root cap; CE, cell elongation; RH, root hair; CS, endodermal cells with casparian strip; PM, proximal meristem; M, meristem (SCN and PM). Each dot denotes a single cell. Colors denote corresponding cell clusters as shown in **(A)**.

(D) Spatial distribution of cell clusters in *Arabidopsis* root. Colors denote corresponding cell clusters as shown in **(A)**.

cell-to-cell movement, with highest level at root tip (Mahonen et al., 2014). The PLT gradient coordinates with root cell division, growth, and differentiation by activating cell division and growth-related genes and repressing differentiation genes (Santuari et al., 2016). More recently, it was revealed that the spatial distribution of auxin and cytokinin, in coordination with PHLOEM EARLY DOF (PEAR) and microRNA165/6-targeted HD-ZIP III transcription factors, forms a regulatory network in regulating cambium stem cell population and procambium cell development (Miyashima et al., 2019; Smetana et al., 2019).

Using cell-type-specific reporter lines in combination of cell sorting, microarray, and RNA sequencing, previous studies have revealed the specific expression patterns of 14 nonoverlapping root cell types in *Arabidopsis* (Birnbaum et al., 2003; Brady et al., 2007; Li et al., 2016). Interestingly, transcriptional similarity between disparate cell types and expression fluctuation along root developmental axis were observed. However, it is still unclear whether all the cell types in roots have been identified. In addition, whether the cells within a given cell type are homogeneous or heterogeneous remains to be clarified. Furthermore, the identification of cell identity of each cell undergoing differentiation and reconstruction of the hierarchical structure in roots has not been reported.

Recent advances in single-cell RNA sequencing (scRNA-seq) technology provide unprecedented opportunities to systematically identify the entire cellular and molecular differentiation trajectory of stem cells at the single-cell level (Islam et al., 2014; Macosko et al., 2015). Whereas initial studies only analyzed fewer than 100 single cells, a series of technological advances, including robotics, microfluidics, and hydrogel droplets, increases the throughput of assays to tens of thousands of cells per experiment (Jaitin et al., 2014; Shalek et al., 2014; Treutlein et al., 2014; Satija et al., 2015). Importantly, a number of algorithms have been developed to decode the cellular regulatory codes from scRNA-seq datasets (Trapnell et al., 2014; Haghverdi et al., 2015, 2016; Satija et al., 2015; Aibar et al., 2017; Becht et al., 2019). For example, the spatial reconstruction of single-cell gene expression data is achieved by Seurat, whereas Monocle 2 has been widely used for inferring the developmental trajectories (Satija et al., 2015; Qiu et al., 2017).

Here, we investigated gene expressions of thousands of *Arabidopsis* root cells at the single-cell level. We found that root cells are highly heterogeneous, even within a single cell type. In combination with pseudo-time analyses, the single-cell root cell atlas was able to reconstruct continuous trajectory of root cell differentiation. We have developed an online web server (http://wanglab.sippe.ac.cn/rootatlas/) to facilitate the use of the datasets generated in this study. The hundreds of identified cluster-specific marker genes also provide a valuable resource for root biology research.

RESULTS

scRNA-Seq and Identification of Root Cell Clusters

To perform scRNA-seq of *Arabidopsis* root cells, we harvested root tissues (0.5 cm in length from root tip, n = 85 roots) and digested them into protoplasts (plant cells without cell wall) (Supplemental Figure 1). About 15 000 cells were initially mixed with 10xGenomics single-cell reaction regents for scRNA-seq assay. The DNA-sequencing libraries were constructed and sequenced by Illumina NovaSeq sequencer. Data were prefiltered at both cell and gene level, resulting in a pool of 7695 cells with 23 161 genes used for further analysis (see Methods). Using linear dimensional reduction, the scaled data were reduced into 100 approximate principal components (PCs) (Becht et al., 2019). The *t*-distributed stochastic neighborhood embedding (*t*-SNE) tool was used to visualize and explore the datasets (van der Maaten and Hinton, 2008). These unsupervised analyses (i.e., no prior knowledge of cell population markers is required to drive clustering) grouped root cells into 24 cell clusters (Figure 1A). A series of specific marker genes (specifically expressed in one or two clusters, see Methods) for each cluster was identified (Supplemental Figures 2 and 3; Supplemental Table 1). To annotate these clusters, we used more than 103 cluster marker genes whose functions and expression patterns have been well studied (Supplemental Table 2). By correlation coefficiency analysis between the cluster-enriched genes and published root cell-type expression profiles (Supplemental Figure 4) (Brady et al., 2007; Li et al., 2016), the cell type of each cluster was further validated. The representative cluster marker genes included stele genes *SUCROSE-PROTON SYMPORTER 2* (*SUC2*) and *TARGET OF MONOPTEROS 5* (*TMO5*) (De Rybel et al., 2014; Wu et al., 2016), root cap gene *ARABIDOPSIS NAC DOMAIN CONTAINING PROTEIN 33* (*ANAC033*) (Bennett et al., 2010), root hair gene *COBRA-LIKE 9* (*COBL9*) (Kamiya et al., 2016), phloem gene *PHLOEM PROTEIN 2-A1* (*ATPP2-A1*) (Cayla et al., 2015), endodermal gene *MYB DOMAIN PROTEIN36* (*MYB36*) which promotes the development of casparian strip (Kamiya et al., 2015; Liberman et al., 2015), meristematic genes *ROOT MERISTEM GROWTH FACTOR 2* (*RGF2*) and *PLT1* (Aida et al., 2004; Matsuzaki et al., 2010; Fernandez et al., 2013), xylem gene *IRREGULAR XYLEM 9* (*IRX9*) (Pena et al., 2007), epidermis genes *PROTODERMAL FACTOR 1* (*PDF1*) and *MERISTEM LAYER 1* (*ATML1*) (Abe et al., 2001; Meyer et al., 2017), lateral root gene *LIKE AUX1 3* (*LAX3*) (Swarup et al., 2008), and photosynthetic genes *PHOTOSYSTEM I LIGHT HARVESTING COMPLEX GENE 1* (*LHCA1*) and *PHOTOSYSTEM I LIGHT HARVESTING COMPLEX GENE 2* (*LHCA2*) (Huang et al., 2017). These marker genes were highly and specifically enriched in each corresponding cluster (Figure 1B; Supplemental Table 1; Supplemental Figures 3 and 5).

We noted three interesting aspects from cell-clustering analyses. First, we found that the specialized cells such as xylem (cluster 15), phloem (cluster 9), endodermal cells with casparian strip (cluster 10 and 22), epidermis (cluster 18), and root hair (cluster 8 and 17) exhibited relatively distinct transcriptome profiles. The cell clusters of these cell types were scattered on the *t*-SNE plot while other cell clusters were grouped together (Figure 1A). Second, we found that a given root cell type may consist of different subpopulations. For example, clusters 1 and 7 belonged to phloem/pericycle cells, suggesting that phloem/pericycle cells are unexpectedly heterogeneous, with at least two subcell types. Consistent with this, gene ontology (GO) analysis demonstrated that cluster 1 showed gene signature for ‘‘organophosphate’’ and ‘‘amino acids catabolic

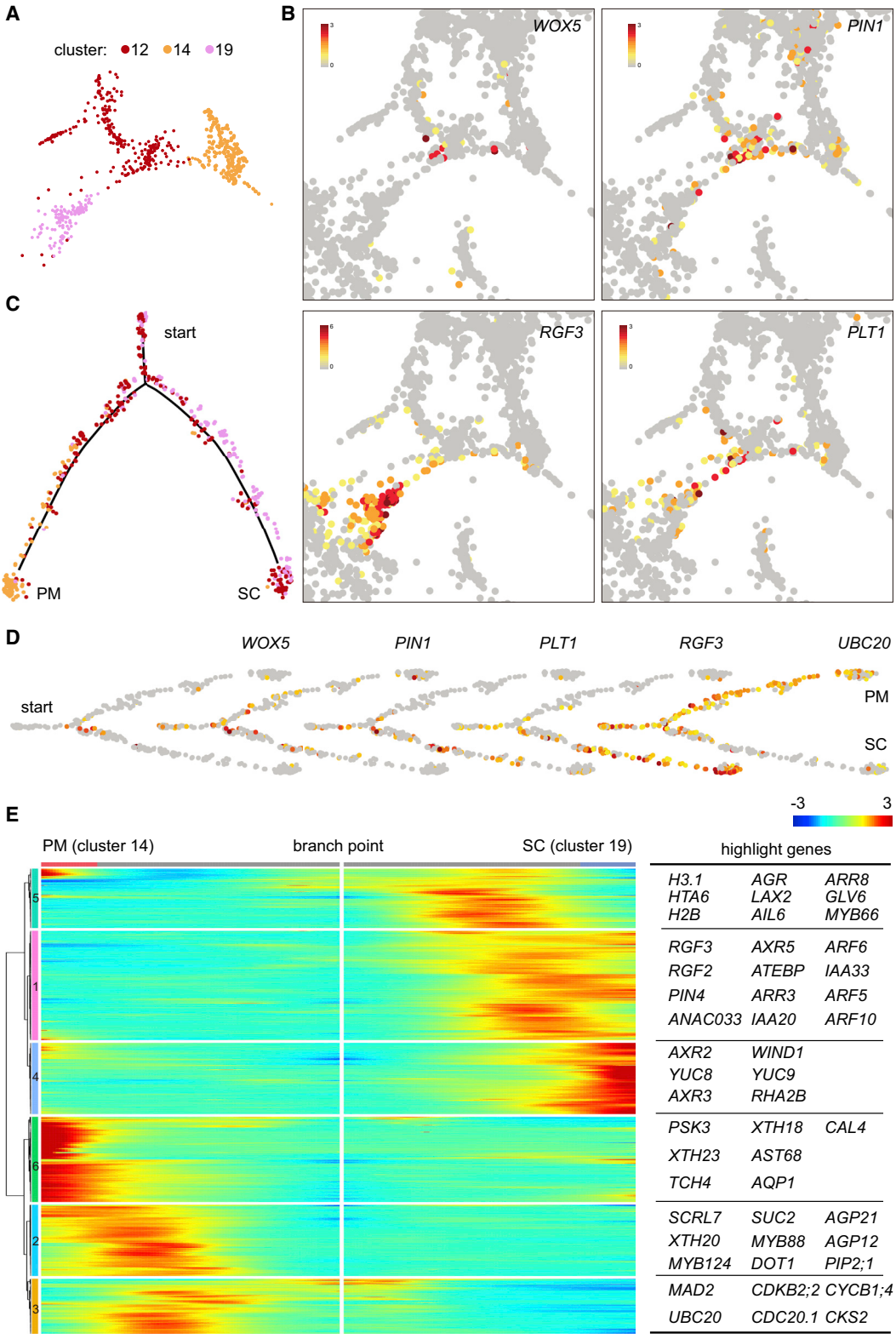

Figure 2. Differentiation Trajectory of Proximal Meristem.

(A) UMAP visualization of SCN and PM (clusters 12, 14, and 19). Each dot denotes a single cell.

(B) Expression patterns of root meristematic genes (*WOX5*, *PIN1*, *RGF3*, and *PLT1*). The colors represent expression levels of these genes in individual cells on the UMAP plot. Color bar indicates the relative expression level.

(legend continued on next page)

process,'' whereas the genes highly expressed in cluster 7 were involved in ''RNA modification'' and ''ribonucleotide metabolic process'' (Supplemental Table 3). Similarly, even though both clusters 10 and 22 were enriched in casparian strip regulatory gene *MYB36*, the genes related to cell wall biosynthetic pathway were only overrepresented in cluster 10. By contrast, biological processes involved in ''endomembrane system organization'' and ''ion transport'' were predominantly represented in cluster 22 (Supplemental Table 3). It is likely that cluster 22 represents an intermediate state of endodermis during the development of casparian strip. Alternatively, these cells might form a novel cell type within the endodermis. In favor of this hypothesis, a recent study has shown that passage cells, a population of interspersed unsuberized cells, exist in suberized endodermis (Andersen et al., 2018). Third, we identified several putative novel cell/subcell types in roots (clusters 6, 11, 16, 17, 22, and 24). In particular, we found that cluster 24 was enriched for the genes involved in photosynthesis, suggesting that some root cells may have photosynthetic potential as mesophyll cells. Clusters 6 and 11 could not be termed because of the lack of proven marker genes. Examination of the enriched genes within these clusters revealed that the extensin genes such as *EXTENSIN 1* (*EXT1*) and *EXT3* were highly expressed in both clusters (Supplemental Table 1), implying that the cells of these two cell types may undergo cell elongation. Taken together, these results reveal the high degree of cell heterogeneity in *Arabidopsis* root and identify a set of putative novel cell types.

Reconstruction of the Continuous Differentiation Trajectory of Root Cells from a Single-Cell Snapshot

Since the cells in the intermediate states (i.e., the cells undergoing the transition from one to another state) could be captured, scRNA-seq enables the exploration of the continuous differentiation trajectory of a developmental process (Bendall et al., 2014; Trapnell et al., 2014; Haghverdi et al., 2015; Tusi et al., 2018; Zhong et al., 2018). To this end, we used the uniform manifold approximation and projection (UMAP) algorithm to visualize the closest possible equivalent fuzzy topological structure of each major cluster (Becht et al., 2019). Although the cell clusters remained similarly identifiable in UMAP as compared with *t*-SNE (Figure 1A and 1C), the hierarchical structures of between cell clusters were clearly identified by UMAP (Figure 1C). The clusters corresponding to root meristematic cells (clusters 12, 14, and 19) were located in the center region (Figure 1C). Notably, UMAP revealed two continuous trajectories of root development based on this niche: one led to the differentiation of root cap, lateral root cap, epidermis, and root hairs toward distal end and another led to the differentiation of multiple stele cell types toward the proximal end. Moreover, the projection of cell clusters onto root architecture mimicked the de facto developmental map of root (Figure 1D).

The clusters 2, 8, 9, 10, 17, 22, and 24 were scattered on UMAP, probably because the cells from these clusters were terminally differentiated with specialized transcriptional profiles. Intriguingly, the distinct cell clusters may share the similar biological processes. For instance, both endodermis with casparian strip cluster (clusters 10 and 22) and root cap cluster (clusters 4 and 5) were enriched in the genes regulating ''response to wounding,'' ''response to water,'' and ''response to nitrate'' (Supplemental Table 3). As a result, endodermis with the casparian strip cluster were gathered with the root cap cluster, but segregated from the clusters related to stele (Figure 1C).

To order cells along a reconstructed ''trajectory'' of root cell differentiation, we used Monocle 2, an algorithm that uses reversed graph embedding to describe multiple fate decisions in a fully unsupervised manner (Trapnell et al., 2014; Qiu et al., 2017). A small number of the cells from clusters 12 and 19 assembled at the beginning of pseudo-time. The transcription factor *WOX5*, which is required for QC function and stem cell maintenance in RAM (Sarkar et al., 2007), was prominently expressed at the branching point and cluster 12 (Figure 2B and 2D; Supplemental Figure 6). The gene signature of cluster 12 was enriched for functional annotations including ''histone modification'' and ''ribonucleoprotein complex biogenesis'' (Supplemental Table 3), in agreement with published expression profile of QC (Nawy et al., 2005). An auxin maxima at QC and its cells beneath is important for SCN function (Blilou et al., 2005; Grieneisen et al., 2007; Santuari et al., 2016). The genes related to auxin response such as *INDOLE-3-ACETIC ACID INDUCIBLE 33* (*IAA33*), *AUXIN RESPONSE FACTOR 5* (*ARF5*), and *AUXIN RESPONSE FACTOR 10* (*ARF10*), and auxin biosynthesis such as *YUCCA 3* (*YUC3*), *YUC8*, and *YUC9* were enriched in clusters 12 and 19 (Supplemental Table 1). Consistently, the root meristematic genes such as *PLT1*, *RGF2*, and *ROOT MERISTEM GROWTH FACTOR 3* (*RGF3*) were also highly expressed within these two populations (Figures 1B and 2B; Supplemental Figure 7; Supplemental Table 1). Because the cells from both clusters were grouped at one branch with pseudo-time (Figure 3C) and shared similar expression signatures, we assigned clusters 12 and 19 to the SCN. It is likely that QC cells reside in one of these two populations and that the cells of this branch represent a self-renewal state of root stem cell.

Interestingly, cluster 14 was separated from clusters 12 and 19 over pseudo-time (Figure 2C). The embedded heatmap and GO enrichment analyses revealed that the trajectory of cluster 14 started with a high rate of cell division (Figure 2E). The cell-cycle genes such as *UBIQUITIN-CONJUGATING ENZYME 20* (*UBC20*), *MITOTIC ARREST-DEFICIENT 2* (*MAD2*), *CYCLIN-DEPENDENT KINASE B2*;*2* (*CDKB2*;*2*), *CYCLIN B1*;*4* (*CYCB1*;*4*), and *CDK-SUBUNIT 2* (*CKS2*) were actively transcribed. Notably, expression levels of the cell-cycle genes

(C) Simulation of the successive differentiation trajectory of SCN over pseudo-time. ''Start'' denotes the beginning of pseudo-time. Pseudo-time increases along the differentiation trajectory. SC, stem cell; PM, proximal meristem.
(D) Expression patterns of *WOX5*, *PIN1*, *RGF3*, *PLT1*, and *UBC20* over pseudo-time. Root meristematic genes and cell-cycle genes are segregated along differentiation. Color bar indicates the relative expression level. SC, stem cell; PM, proximal meristem.
(E) Heatmap showing the expression of the branch-dependent genes over pseudo-time. The branch point (shown in the middle of heatmap) is the beginning of pseudo-time. Both sides of heatmap are the end of pseudo-time. The representative branch-dependent genes are shown in the table on the right. Color bar indicates the relative expression level. SC, stem cell; PM, proximal meristem.

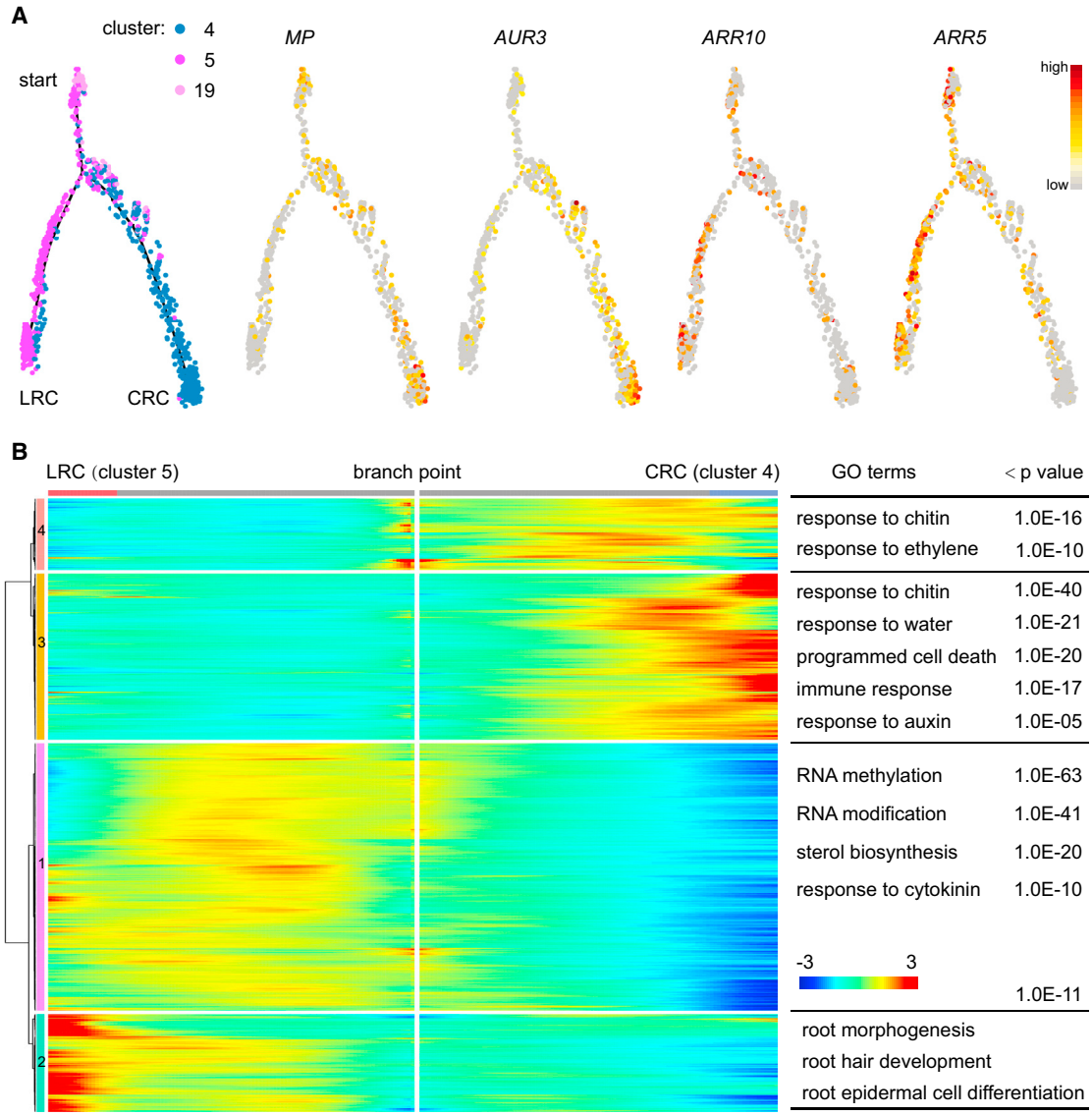

Figure 3. Differentiation Trajectory of Root Cap.

(A) Simulation of the successive differentiation trajectory of root cap and lateral root cap cells by pseudo-time. Expression patterns of representative auxin-related genes (*AUR3* and *MP*) and cytokinin-related genes (*ARR10* and *ARR5*) are shown over the course of pseudo-time. "Start" denotes the beginning of pseudo-time. LRC, lateral root cap; CRC, columella root cap. Color bar indicates the relative expression level.

(B) Heatmap showing the expression of the branch-dependent genes over pseudo-time. Representative GO terms and *p* value of each gene cluster are shown in the table on the right. The branch point (shown in the middle of the heatmap) is the beginning of pseudo-time. Both sides of the heatmap are the end of pseudo-time. Color bar indicates the relative expression level. LRC, lateral root cap; CRC, columella root cap.

decreased over pseudo-time (Figure 2E). We noted that two closely related MYB transcription factors, *MYB88* and *MYB124*, were highly expressed at this stage (Figure 2E). Previous studies have shown that MYB88 and MYB124 collaboratively inhibit cell division by repressing *CDKB1;1* (Yang and Sack, 1995; Lai et al., 2005; Xie et al., 2010). Thus, a plausible explanation for this observation is that *MYB88* and *MYB124* are responsible for halting cell division, which subsequently facilitates cell differentiation. In agreement with this hypothesis, the genes involved in cell elongation and expansion including *ARABINOGALACTAN PROTEIN 12* (*AGP12*), *ARABINOGALACTAN PROTEIN 21* (*AGP21*), *XYLOGLUCAN ENDOTRANSGLUCOSYLASE/HYDROLASE 20* (*XTH20*), and *PLASMA MEMBRANE INTRINSIC PROTEIN 2* (*PIP2.1*) were accordingly increased at a later stage (Figure 2E). Therefore, the gene signatures and differentiation trajectory suggest that cluster 14 behaves as proximal meristem (PM) (Bennett and Scheres, 2010; Del Bianco et al., 2013). The ordering of the cells of this cluster reconstructs the progression of cell-fate determination at the PM region (Dolan et al., 1993; Ohashi-Ito and Bergmann, 2007; Aichinger et al., 2012).

Root cap protects root tip and plays an important role in nutrient assimilation and environmental sensing. The epidermal/lateral root cap initials give rise to epidermis and lateral root cap, while the columella initials contribute to columella root cap formation

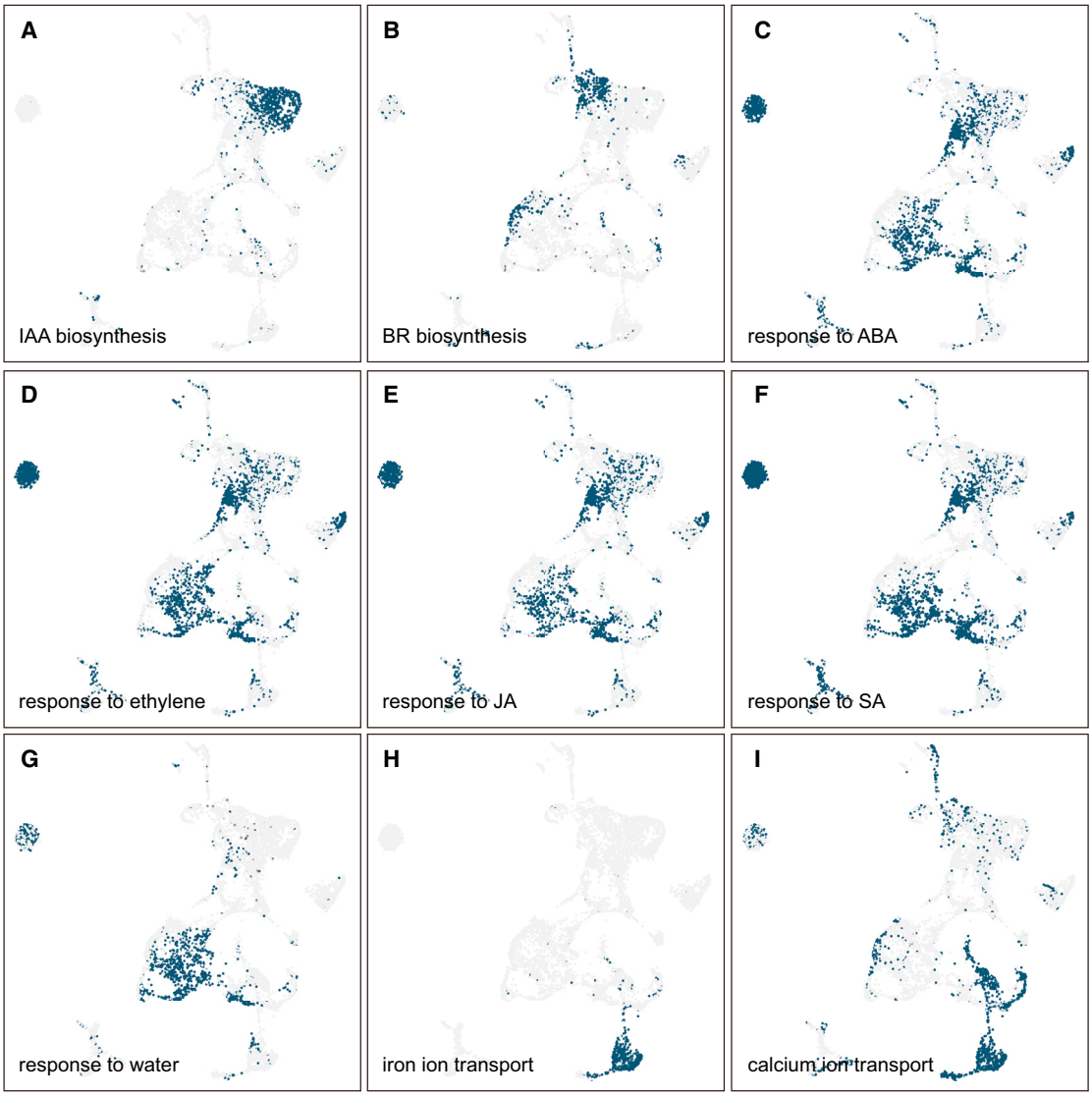

Figure 4. Distinct Pattern of Ion Assimilation and Hormonal Response.
Expression patterns of the genes related to hormone biosynthesis **(A and B)**, hormone response **(C–G)**, and ion assimilations **(H and I)**. The colors represent high expression levels of these genes in individual cells on the UMAP plot.

(Aichinger et al., 2012). To trace their differentiation trajectories, we applied pseudo-time analysis to the cells from clusters 4, 5, and 19. Consistent with aforementioned data, the differentiation started with cluster 19 (Figure 3A). Over pseudo-time, the trajectory of these cells bifurcated into two distinct orientations (columella root cap and lateral root cap) (Figure 3A). Importantly, the cells from cluster 5 were grouped into the lateral root cap (LRC) branch, whereas those from cluster 4 were grouped into the columella root cap (CRC) branch. Signature genes of the CRC branch were enriched for "response to chitin," "response to water," "programmed cell death," and "immune response" based on functional enrichment analysis (Figure 3B). Signature genes of the LRC branch were initially enriched for functional annotations including "RNA methylation and modification" and "sterol biosynthesis," and eventually enriched for the genes involved in root epidermal cell differentiation and root hair development (Figure 3B). This trajectory supports the notion that LRC, epidermis, and root hair originate from the epidermal/lateral root cap initials (Dolan et al., 1993; Aichinger et al., 2012). Taken together, the above results demonstrate that scRNA-seq enables us to reconstruct the continuous differentiation trajectory of root cells and to investigate the cell transcriptome profiles in the intermediate state during cell differentiation.

Differential Hormonal Response and Ion Assimilation Pattern in Root Cell Atlas

Plant hormones are important for root development and stress response. We plotted the genes related to hormone biosynthesis, transport, and response on UMAP. Interestingly, we found that the genes involved in indole-3-acetic acid (an auxin) biosynthesis were highly enriched in cluster 1 (Figure 4A), whereas the genes related to brassinosteroid biosynthesis were overrepresented in

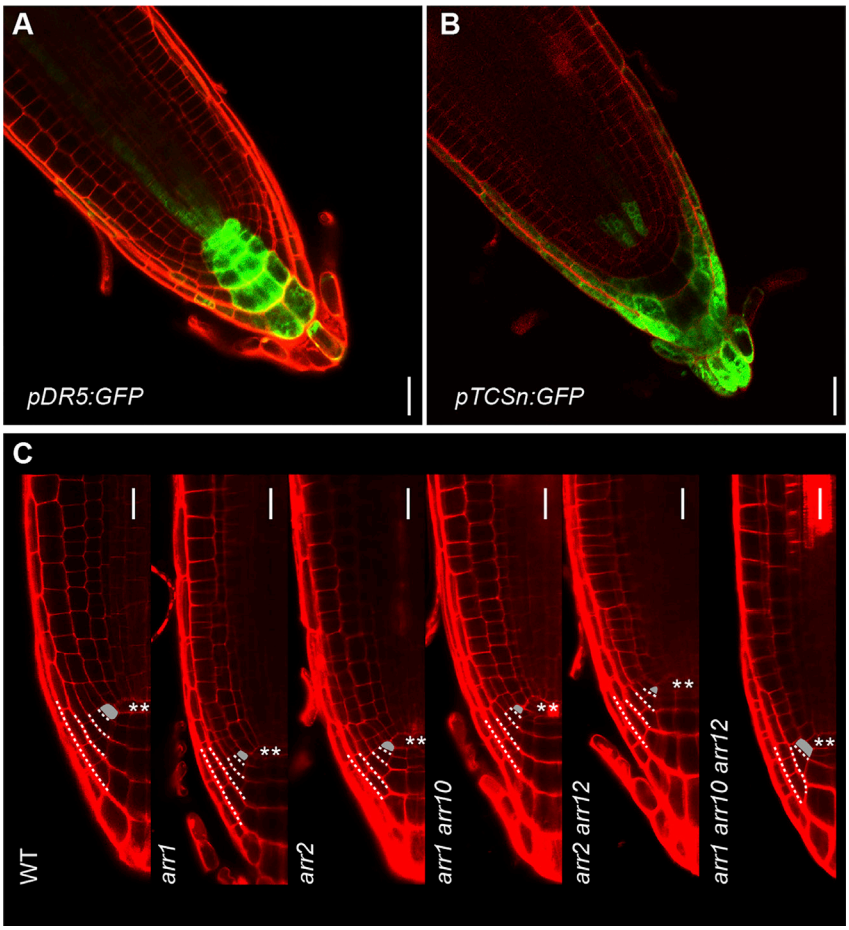

Figure 5. Regulation of Lateral Root Cap Development by Cytokinin.

(A and B) Expression pattern of *pDR5*:*GFP* (**A**, green) and *pTCSn*:*GFP* (**B**, green) in *Arabidopsis* root tip. Cell outlines were stained by propidium iodide (red). Scale bars, 20 μm.

(C) Phenotypes of wild type (WT; Col-0), *arr1*-3, *arr2*-4, *arr1*-3 *arr10*-5, *arr2*-4 *arr12*-1, and *arr1*-3 *arr10*-5 *arr12*-1 in lateral root cap development. The cell layers of lateral root cap are marked by dotted lines. Gray areas mark the stem cells for the epidermis and lateral root cap. Scale bars, 20 μm. ** stands for QC.

cluster 7 (Figure 4B). Because both clusters 1 and 7 were assigned as phloem/pericycle, these results imply that the subcell types of phloem/pericycle are functionally specified in terms of hormone biosynthesis. The distribution pattern of eight *PIN-FORMED* (*PIN*) genes, which are involved in auxin polar transport (Barbosa et al., 2018), was largely consistent with published data (Supplemental Figure 8) (Feraru and Friml, 2008; Omelyanchuk et al., 2016). Abscisic acid, ethylene, jasmonic acid, and salicylic acid are four major hormones in response to stress. All of these hormones showed a similar pattern, with highest response in cluster 4 (CRC) and cluster 13 (endodermis) (Figure 4C–4F).

Root cells are responsible for water uptake, nutrition, and ion assimilation in plants. The genes with annotation of "response to water" were enriched in cluster 4 (CRC) (Figure 4G), supporting a role of root cap in water sensing and hydrotropism (Takano et al., 1995). Intriguingly, the genes related to iron (Fe) and calcium (Ca) transport were predominantly expressed in clusters 8 and 17 (root hair, Figure 4H and 4I). In agreement with this, a very recent report has revealed that root hair abundance is positively correlated with the accumulation of cadmium, another bivalent ion (Kohanova et al., 2018). Taken together, these results illustrate that a single-cell root cell atlas is powerful for functional dissection of the biological processes related to hormonal response and ion assimilation at single-cell resolution.

Identification of a Role of Cytokinin Response in Lateral Root Cap Development

We observed the partition of cytokinin and auxin signaling pathway along root cap and LRC differentiation trajectories. The auxin-related genes including *AUXIN UPREGULATED 3* (*AUR3*) and *MONOPTEROS* (*MP*/*ARF5*) (Normanly et al., 1997; Staswick et al., 2005; Schlereth et al., 2010; Rademacher et al., 2011; Chen et al., 2014) were enriched in the CRC branch (Figure 3A and Supplemental Figure 9). In contrast, the cytokinin pathway genes such as *ARABIDOPSIS THALIANA RESPONSE REGULATOR 5* (*ARR5*), *ARR6*, *ARR8*, *ARR10*, and *HISTIDINE-CONTAINING PHOSPHOTRANSMITTER3* (*AHP3*) (Hwang et al., 2012) were highly expressed in the LRC branch (Figure 3A and Supplemental Figure 10). Over pseudo-time, cytokinin response was prominent before the cells became fully differentiated (Figure 3B). Interestingly, these results were consistent with previous observation using synthetic auxin and cytokinin reporters, *pDR5*:*GFP* and *pTCSn*:*GFP*, respectively (Sabatini et al., 1999; Zurcher et al., 2013).

The LRC is derived from the epidermal (Epi) lineage by periclinal divisions of epidermal/lateral root cap initials (Dolan et al., 1993). LRC daughter cells undergo several rounds of anticlinal divisions to extend the cell file before differentiating. In the wild type, four LRC cell layers were observed (Figure 5C). The LRC cell layers of single and double mutants of *B-ARR* did not differ from those of wild type. However, *arr1 arr10 arr12* triple mutant, which was largely defective in cytokinin signaling output, showed a reduced number of LRC cell layers (Figure 5C). Thus, these results demonstrate the functional significance of high cytokinin response during root epidermal cell differentiation and LRC development.

DISCUSSION

scRNA-seq is a powerful tool to reveal cellular heterogeneity, discover new cell types, and characterize the developmental trajectory. It should be noted that high-throughput application of scRNA-seq to solid plant tissues relies on dissociating tissues or organs into single cells, separating cells from their native

spatial context such that further analyses lack crucial information on cells' environments and locations. To circumvent this problem, Seurat, a computational strategy, has been widely used to identify cell clusters, localize rare cell populations, and map both spatially restricted and scattered groups (Satija et al., 2015). Moreover, the subsequent analysis with Monocle 2 leads to the reconstruction of a continuous differentiation trajectory in diverse systems (Qiu et al., 2017). However, these *in silico* predictions have to be carefully validated by other experimental approaches such as promoter reporter analysis and cell-lineage tracing. Alternatively, the development of a toolbox for imaging gene expression in single cells will ultimately reveal the spatiotemporal regulation of gene expression in any biological processes (Pichon et al., 2018).

Similar to the Human Cell Atlas Project, the Plant Cell Atlas Project (PCA), which aims to dissect plant development at single-cell resolution, has been recently proposed (Rhee et al., 2019). Generation of a fundamental framework for PCA requires construction of the single-cell transcriptome profiles for each cell type in plants. Our results, together with the datasets generated by the labs of Cuperus, Timmermans, and Schiefelbeins, now uncover the cellular heterogeneity in *Arabidopsis* root at highest resolution (Denyer et al., 2019; Jean-Baptiste et al., 2019; Ryu et al., 2019). The numbers of cells captured in these independent scRNA-seq experiments varied. As a result, the numbers of cell clusters identified were also different. Notably, given the same sequencing depth and parameters used in Seurat, the cluster number is positively correlated with the number of sequenced cells. Moreover, the increased number of cells in the intermediate state could further facilitate the reconstruction of a faithful differentiation trajectory. Thus, the integration of different scRNA-seq datasets deposited in public repositories and generation of a web server for comparative analysis might be an important future direction.

The preparation of sufficient single cells for scRNA-seq is still challenging in plants. Protoplasting is widely used for dissociating plant tissues. However, the treatment time has to be optimized according to the tissues of origin. In addition, we observed a tradeoff between treatment time and the quality of single-cell suspension. The rare cell types such as the endodermal cells with casparian strip and $WOX5^+$ (WOX5-positive) cells with short reaction time could not be efficiently captured and reconstructed in the cell atlas. By contrast, a longer enzymatic digestion usually leads to a reduction in cell viability and RNA abundance. Based on our pilot experiments, we found that 2 h of treatment for protoplasting is an optimal condition for root scRNA-seq with more than 85% of viable cells being retrieved. Moreover, an RNase-free condition during protoplasting is also recommended. scRNA-seq could be further optimized at the data-analysis stage. For example, the dead cells and the genes only expressed in a few cells are filtered out. The genes with low dispersion, such as housekeeping genes, are not included for cell clustering and other downstream analyses.

Collectively, our study illustrates the power of scRNA-seq for dissection of cellular heterogeneity and the developmental trajectory in plants. The identified cell clusters, together with cluster-specific marker genes, pave the way for us to analyze the developmental and physiological function of the novel cell types in roots. More importantly, expression profiling of thousands of the cells undergoing differentiation enables us to reconstruct the continuous differentiation trajectories of any root cell type at the single-cell level. Due to the low number of QC cells in roots, we were unable to faithfully identify a corresponding cell cluster in our scRNA-seq dataset. Thus, the combination of scRNA-seq with cell-type marker-based cell-sorting technology may help us to investigate the maintenance and differentiation of rare cell types in plants in the future.

METHODS

Plant Materials and Growth Conditions

The wild-type *A. thaliana* (ecotypes Col-0) was used for root scRNA-seq experiments. Seeds were sterilized with 15% bleach and germinated on vertical half-strength Murashige and Skoog (1/2 MS) plates (2.21 g of MS basal medium with vitamin powder and 8 g/l agar, pH 5.7) at 21°C (day)/19°C (night) in long-day conditions (16 h light/8 h dark, with a light intensity of 80 mmol/m^2/s using Philips TLD 36W/865 and 36W/830 bulbs). The root tissues were harvested after 10 days of growth. *arr1*-3, *arr2*-4, *arr1*-3 *arr10*-5, *arr2*-4 *arr12*-1, *arr1*-3 *arr10*-5, *arr12*-1, *pDR5*:*GFP*, and *pTCSn*:*GFP* were described previously (Sabatini et al., 1999; Leibfried et al., 2005; Mason et al., 2005; Zurcher et al., 2013; Zhang et al., 2017). For root phenotypic assays, the seeds were sterilized and germinated on 1/2 MS vertical plates.

Preparation of Root Samples for scRNA-seq

The root tip regions (0.5 cm in length from root tip) were harvested and digested for 2 h at room temperature in RNase-free enzyme solution (1.5% cellulase R10, 1.5% macerozyme R10, 0.4 M mannitol, 10 mM KCl, 10 mM $CaCl_2$ and 0.1% BSA). The protoplasts were filtered with a cell strainer (40 μm diameter, Falcon #352340), concentrated, and washed three to four times with 8% mannitol at room temperature. Protoplast viability was determined by trypan blue staining, with the ratio of viable cells being more than 85%. The concentration of protoplasts was adjusted to 1500–2000 cells/μl. The cells were then processed with the 10xGenomics Single Cell Protocol (CG00052, RevC).

scRNA-Seq Library Construction and Sequencing

Approximately 15 000 counted cells were loaded on Single Cell A Chip. The libraries were constructed using Chromium Controller and Chromium Single Cell 3′ Reagent Kits v2. In brief, cell suspensions in a chip were loaded on a Chromium Controller (10xGenomics, Pleasanton, CA) to generate single-cell GEMs (gel beads in emulsion). scRNA-seq libraries were then prepared using the Chromium Single Cell 3′ Gel Bead and Library Kit (P/N #120236, 120237, 120262; 10xGenomics). Qualitative analysis of DNA library was performed by an Agilent 2100 Bioanalyzer. The concentration of DNA library was measured by Qubit (Invitrogen). Libraries were sequenced by an Illumina NovaSeq sequencer (Genergy Biotechnology Shanghai). The raw scRNA-seq dataset comprised Read1, Read2, and i7 index read. The 26-bp read length of Read1 contained the sequence of the 16 bp 10xBarcode and 10 bp UMI (unique molecular identifiers). The 98-bp read length of Read2 was the sequence of the cDNA fragment. In total, 317 339 569 reads were obtained.

Pre-processing of Raw scRNA-Seq Data

The raw scRNA-seq dataset was first analyzed by Cell Ranger 2.2.0 (10xGenomics). These pipelines include processing of raw scRNA-seq data to align reads and generate gene-cell matrices. The genome and GTF annotation files of *A. thaliana* were downloaded from the TAIR10 website (https://www.arabidopsis.org/). Note that the version of genome was TAIR10 and the version of annotation files was Araport11 (downloaded from https://www.arabidopsis.org/). Run 'cellranger mkref' with "–genome, –fasta and –genes" arguments to build reference. Run 'cellranger count' with "–id, –transcriptome, –fastqs, –sample and –force-cells = 8000"

arguments to generate single-cell gene counts. 91.7% reads were aligned to the TAIR10 reference genome by the aligner STAR (v.2.5.1b) (Dobin et al., 2013). Mean reads per cell were 39 667. Median genes per cell were about 1875. The gene-cell matrices (named 'filtered_gene_bc_matrices' by 10xGenomics) generated by Cell Ranger 2.2.0 served as raw data for further analyses.

Gene-Overlapping Analysis

The published RNA-seq data of 14 GFP marker lines (Li et al., 2016) were downloaded from NCBI (PRJNA323955: SRR3664374-SRR3664437). Salmon (Patro et al., 2017) was used to quantify transcript abundances. The whole transcriptome of *A. thaliana* was downloaded from Araport11 (www.araport.org). Run 'salmon index' with "-t, -i, –type quasi, -k 31" arguments to build the index of *A. thaliana* transcriptome. The expression level of each gene was quantified using 'salmon quant' with "-i, -l A, -1, -2" arguments. Each output file (named "quant.sf") contained the name of each transcript, its length, effective length, its abundance in terms of transcripts per million, and estimated number of reads. These data were then loaded into DESeq2 (Love et al., 2014) for measuring differential expression. To identify specifically expressed genes in each marker lines, one marker line served as "treatment" while the other was assigned as "control". The highly enriched genes ($\log_2$ fold change $\geq$1.0) of each marker line were selected for overlapping analyses with cluster-enriched genes.

Cell Clustering and Reconstruction of Cell Trajectories by Nonlinear Dimensional Reduction

The gene-cell matrices (named 'filtered_gene_bc_matrices' by 10xGenomics) of 8000 cells were load into the Seurat package (v. 3.0.0.9), which was implemented in R (v. 3.5.1). To remove dead cells and doublets, we filtered the cells with unique gene counts over 5000 or fewer than 500. The cells with more than 5% mitochondrial sequence were also removed. The genes expressed in at least three single cells were kept. After filtering, 23 161 genes across 7695 cells were used for downstream analysis. The scaled data were first normalized by 'LogNormalize.' We then used 'FindVariableFeatures' with "mean.cutoff (0.0125–3) and dispersion.cutoff (1.5, Inf)" parameters to calculate highly variable genes. A total of 1308 genes were used for clustering analysis. For PC analysis, the scaled data were reduced to 100 approximate PCs depending on the 1308 highly variable genes (set npcs = 100). Clusters were identified using the Seurat function 'FindClusters' with "resolution = 1.0." The data structures and cell trajectories were separately visualized and explored by *t*-SNE (run the 'RunTSNE' function with "dims = 40") and UMAP (run the 'RunUMAP' function with "'n.neighbors = 30', 'metric = correlation,' and 'min.dist = 0.3'"). Cluster marker genes (cluster-enriched genes) were identified using Seurat function 'FindAllMarkers' and tested by 'roc.' The cluster-enriched genes were detected by parameters of "min.pct = 0.25" and "logfc.threshold = 0.58," which means the minimum cell percentage for marker genes is more than 0.25 and the $\log_2$ fold change of average expression is more than 0.58. Cluster-specific marker genes were selected from among 6714 cluster-enriched genes based on the criteria that marker genes must be expressed in 25% of cells of a cluster and enriched in one or two clusters. The repeated analysis has been performed many times with the same or different parameters.

Pseudo-Time Analysis

The Monocle (v.2.8.0) package was used to deeply analyze the process of cell differentiation and the determination of cell fate. To explore related clusters, we extracted the subset of raw data with cluster information. First, run 'dispersionTable' to calculate the variance in each gene's expression across cells. Based on average expression level (the "mean_expression" parameter), variable genes were chosen to define a developmental progress. Second, the data's dimensionality was reduced to two components (set "max_components = 2, method = 'DDRTree'"). With the expression data in a lower dimensional space, the cells' transition from one state to another was described by 'orderCells'. Call 'orderCells' to order the cells in pseudo-time. The cell trajectory was plotted by 'plot_cell_trajectory' in Monocle. For specifying a priori "beginning" of the trajectory of the tree, run 'orderCells' again setting the "root_state" argument. The branch point was selected to analyze branches in differentiation trajectories. BEAM was used to analyze the pseudo-time-dependent or branch-dependent genes. The genes that were significantly branch-dependent were visualized by the 'plot_genes_branched_heatmap' function. The data used for plotting heatmap were also used for GO biological process analyses.

Pathway Analysis

All differently expressed genes including cluster-enriched genes and branch-dependent genes with statistical significance were applied to clusterProfiler for pathway enrichment analysis (Yu et al., 2012). The pathway enrichment with high statistical significance was annotated to a biological process. To analyze the distribution map of hormone response and transporter, we selected the genes enriched in the same GO terms. The expression levels of the selected genes were summarized and the top 20% of the cells with high expression levels were visualized on UMAP.

Microscopy

To observe the root tips of *arr1*-3, *arr2*-4, *arr1*-3 *arr10*-5, *arr2*-4 *arr12*-1, *arr1*-3 *arr10*-5 *arr12*-1, *pDR5*:*GFP*, and *pTCSn*:*GFP*, we stained roots with propidium iodide (10 μg/ml). The fluorescence signal was observed under a Leica TCS SP8 STED 3X confocal microscope. For GFP, excitation light wavelength was 488 nm and emission was 510–550 nm; for propidium iodide, excitation light wavelength was 561 nm and emission was 631–690 nm.

ACCESSION NUMBERS

The scRNA-seq data used in this study have been deposited in the NCBI SRA database with BioProject number PRJNA517021 and a supplementary web server (http://wanglab.sippe.ac.cn/rootatlas/).

SUPPLEMENTAL INFORMATION

Supplemental Information is available at *Molecular Plant Online*.

FUNDING

This work was supported by grants from the National Key Research & Development Program (2016YFA0500800), National Natural Science Foundation of China (31430013; 31222029; 912173023, 31525004), Strategic Priority Research Program of the Chinese Academy of Sciences (XDB27030101), Young Elite Scientists Sponsorship Program by CAST (2016QNRC001), National Postdoctoral Program for Innovative Talents (BX201600178), and the Sanofi-SIBS 2017 Post-doctoral Fellowship.

AUTHOR CONTRIBUTIONS

T.-Q.Z. and J.-W.W. designed the research. T.-Q.Z. and Z.-G.X. performed research. T.-Q.Z. performed bioinformatics analysis. T.-Q.Z., Z.-G.X., G.-D.S., and J.-W.W. analyzed the data. T.-Q.Z. and J.-W.W. wrote the manuscript.

ACKNOWLEDGMENTS

No conflict of interest declared.

Received: February 6, 2019
Revised: March 29, 2019
Accepted: April 12, 2019
Published: April 17, 2019

REFERENCES

Abe, M., Takahashi, T., and Komeda, Y. (2001). Identification of a cis-regulatory element for L1 layer-specific gene expression, which is targeted by an L1-specific homeodomain protein. Plant J. **26**:487–494.

Aibar, S., Gonzalez-Blas, C.B., Moerman, T., Huynh-Thu, V.A., Imrichova, H., Hulselmans, G., Rambow, F., Marine, J.C., Geurts, P., Aerts, J., et al. (2017). SCENIC: single-cell regulatory network inference and clustering. Nat. Methods **14**:1083–1086.

Aichinger, E., Kornet, N., Friedrich, T., and Laux, T. (2012). Plant stem cell niches. Annu. Rev. Plant Biol. **63**:615–636.

Aida, M., Beis, D., Heidstra, R., Willemsen, V., Blilou, I., Galinha, C., Nussaume, L., Noh, Y.S., Amasino, R., and Scheres, B. (2004). The PLETHORA genes mediate patterning of the *Arabidopsis* root stem cell niche. Cell **119**:109–120.

Andersen, T.G., Naseer, S., Ursache, R., Wybouw, B., Smet, W., De Rybel, B., Vermeer, J.E.M., and Geldner, N. (2018). Diffusible repression of cytokinin signalling produces endodermal symmetry and passage cells. Nature **555**:529–533.

Barbosa, I.C.R., Hammes, U.Z., and Schwechheimer, C. (2018). Activation and polarity control of PIN-FORMED auxin transporters by phosphorylation. Trends Plant Sci. **23**:523–538.

Becht, E., McInnes, L., Healy, J., Dutertre, C.A., Kwok, I.W.H., Ng, L.G., Ginhoux, F., and Newell, E.W. (2019). Dimensionality reduction for visualizing single-cell data using UMAP. Nat. Biotechnol. **37**:38–44.

Bendall, S.C., Davis, K.L., Amir el, A.D., Tadmor, M.D., Simonds, E.F., Chen, T.J., Shenfeld, D.K., Nolan, G.P., and Pe'er, D. (2014). Single-cell trajectory detection uncovers progression and regulatory coordination in human B cell development. Cell **157**:714–725.

Benfey, P.N. (2016). Defining the path from stem cells to differentiated tissue. Curr. Top. Dev. Biol. **116**:35–43.

Bennett, T., and Scheres, B. (2010). Root development-two meristems for the price of one? Curr. Top. Dev. Biol. **91**:67–102.

Bennett, T., van den Toorn, A., Sanchez-Perez, G.F., Campilho, A., Willemsen, V., Snel, B., and Scheres, B. (2010). SOMBRERO, BEARSKIN1, and BEARSKIN2 regulate root cap maturation in *Arabidopsis*. Plant Cell **22**:640–654.

Birnbaum, K., Shasha, D.E., Wang, J.Y., Jung, J.W., Lambert, G.M., Galbraith, D.W., and Benfey, P.N. (2003). A gene expression map of the *Arabidopsis* root. Science **302**:1956–1960.

Blilou, I., Xu, J., Wildwater, M., Willemsen, V., Paponov, I., Friml, J., Heidstra, R., Aida, M., Palme, K., and Scheres, B. (2005). The PIN auxin efflux facilitator network controls growth and patterning in *Arabidopsis* roots. Nature **433**:39–44.

Brady, S.M., Orlando, D.A., Lee, J.Y., Wang, J.Y., Koch, J., Dinneny, J.R., Mace, D., Ohler, U., and Benfey, P.N. (2007). A high-resolution root spatiotemporal map reveals dominant expression patterns. Science **318**:801–806.

Cayla, T., Batailler, B., Le Hir, R., Revers, F., Anstead, J.A., Thompson, G.A., Grandjean, O., and Dinant, S. (2015). Live imaging of companion cells and sieve elements in *Arabidopsis* leaves. PLoS One **10**:e0118122.

Chen, Q., Dai, X., De-Paoli, H., Cheng, Y., Takebayashi, Y., Kasahara, H., Kamiya, Y., and Zhao, Y. (2014). Auxin overproduction in shoots cannot rescue auxin deficiencies in *Arabidopsis* roots. Plant Cell Physiol. **55**:1072–1079.

De Rybel, B., Adibi, M., Breda, A.S., Wendrich, J.R., Smit, M.E., Novak, O., Yamaguchi, N., Yoshida, S., Van Isterdael, G., Palovaara, J., et al. (2014). Integration of growth and patterning during vascular tissue formation in *Arabidopsis*. Science **345**:1255215.

Del Bianco, M., Giustini, L., and Sabatini, S. (2013). Spatiotemporal changes in the role of cytokinin during root development. New Phytol. **199**:324–338.

Denyer, T., Ma, X., Klesen, S., Scacchi, E., Nieselt, K., and Timmermans, M.C.P. (2019). Spatiotemporal developmental trajectories in the *Arabidopsis* root revealed using high-throughput single-cell RNA sequencing. Dev. Cell **48**:840–852.e5.

Dobin, A., Davis, C.A., Schlesinger, F., Drenkow, J., Zaleski, C., Jha, S., Batut, P., Chaisson, M., and Gingeras, T.R. (2013). STAR: ultrafast universal RNA-seq aligner. Bioinformatics **29**:15–21.

Dolan, L., Janmaat, K., Willemsen, V., Linstead, P., Poethig, S., Roberts, K., and Scheres, B. (1993). Cellular organisation of the *Arabidopsis thaliana* root. Development **119**:71–84.

Drapek, C., Sparks, E.E., and Benfey, P.N. (2017). Uncovering gene regulatory networks controlling plant cell differentiation. Trends Genet. **33**:529–539.

Feraru, E., and Friml, J. (2008). PIN polar targeting. Plant Physiol. **147**:1553–1559.

Fernandez, A., Drozdzecki, A., Hoogewijs, K., Nguyen, A., Beeckman, T., Madder, A., and Hilson, P. (2013). Transcriptional and functional classification of the GOLVEN/ROOT GROWTH FACTOR/CLE-like signaling peptides reveals their role in lateral root and hair formation. Plant Physiol. **161**:954–970.

Grieneisen, V.A., Xu, J., Maree, A.F., Hogeweg, P., and Scheres, B. (2007). Auxin transport is sufficient to generate a maximum and gradient guiding root growth. Nature **449**:1008–1013.

Haghverdi, L., Buettner, F., and Theis, F.J. (2015). Diffusion maps for high-dimensional single-cell analysis of differentiation data. Bioinformatics **31**:2989–2998.

Haghverdi, L., Buttner, M., Wolf, F.A., Buettner, F., and Theis, F.J. (2016). Diffusion pseudotime robustly reconstructs lineage branching. Nat. Methods **13**:845–848.

Huang, D., Lin, W., Deng, B., Ren, Y., and Miao, Y. (2017). Dual-located WHIRLY1 interacting with LHCA1 alters photochemical activities of photosystem I and is involved in light adaptation in *Arabidopsis*. Int. J. Mol. Sci. **18**. https://doi.org/10.3390/ijms18112352.

Hwang, I., Sheen, J., and Muller, B. (2012). Cytokinin signaling networks. Annu. Rev. Plant Biol. **63**:353–380.

Islam, S., Zeisel, A., Joost, S., La Manno, G., Zajac, P., Kasper, M., Lonnerberg, P., and Linnarsson, S. (2014). Quantitative single-cell RNA-seq with unique molecular identifiers. Nat. Methods **11**:163–166.

Jaitin, D.A., Kenigsberg, E., Keren-Shaul, H., Elefant, N., Paul, F., Zaretsky, I., Mildner, A., Cohen, N., Jung, S., Tanay, A., et al. (2014). Massively parallel single-cell RNA-seq for marker-free decomposition of tissues into cell types. Science **343**:776–779.

Jean-Baptiste, K., McFaline-Figueroa, J.L., Alexandre, C.M., Dorrity, M.W., Saunders, L., Bubb, K.L., Trapnell, C., Fields, S., Queitsch, C., and Cuperus, J. (2019). Dynamics of gene expression in single root cells of *A. thaliana*. Plant Cell https://doi.org/10.1105/tpc.18.00785.

Kamiya, M., Higashio, S.Y., Isomoto, A., Kim, J.M., Seki, M., Miyashima, S., and Nakajima, K. (2016). Control of root cap maturation and cell detachment by BEARSKIN transcription factors in *Arabidopsis*. Development **143**:4063–4072.

Kamiya, T., Borghi, M., Wang, P., Danku, J.M., Kalmbach, L., Hosmani, P.S., Naseer, S., Fujiwara, T., Geldner, N., and Salt, D.E. (2015). The MYB36 transcription factor orchestrates Casparian strip formation. Proc. Natl. Acad. Sci. U S A **112**:10533–10538.

Kohanova, J., Martinka, M., Vaculik, M., White, P.J., Hauser, M.T., and Lux, A. (2018). Root hair abundance impacts cadmium accumulation in *Arabidopsis thaliana* shoots. Ann. Bot. **122**:903–914.

Lai, L.B., Nadeau, J.A., Lucas, J., Lee, E.K., Nakagawa, T., Zhao, L., Geisler, M., and Sack, F.D. (2005). The *Arabidopsis* R2R3 MYB proteins FOUR LIPS and MYB88 restrict divisions late in the stomatal cell lineage. Plant Cell **17**:2754–2767.

Leibfried, A., To, J.P., Busch, W., Stehling, S., Kehle, A., Demar, M., Kieber, J.J., and Lohmann, J.U. (2005). WUSCHEL controls meristem function by direct regulation of cytokinin-inducible response regulators. Nature **438**:1172–1175.

Li, S., Yamada, M., Han, X., Ohler, U., and Benfey, P.N. (2016). High-resolution expression map of the *Arabidopsis* root reveals alternative splicing and lincRNA regulation. Dev. Cell **39**:508–522.

Liberman, L.M., Sparks, E.E., Moreno-Risueno, M.A., Petricka, J.J., and Benfey, P.N. (2015). MYB36 regulates the transition from proliferation to differentiation in the *Arabidopsis* root. Proc. Natl. Acad. Sci. U S A **112**:12099–12104.

Love, M.I., Huber, W., and Anders, S. (2014). Moderated estimation of fold change and dispersion for RNA-seq data with DESeq2. Genome Biol. **15**:550.

Macosko, E.Z., Basu, A., Satija, R., Nemesh, J., Shekhar, K., Goldman, M., Tirosh, I., Bialas, A.R., Kamitaki, N., Martersteck, E.M., et al. (2015). Highly parallel genome-wide expression profiling of individual cells using nanoliter droplets. Cell **161**:1202–1214.

Mahonen, A.P., Ten Tusscher, K., Siligato, R., Smetana, O., Diaz-Trivino, S., Salojarvi, J., Wachsman, G., Prasad, K., Heidstra, R., and Scheres, B. (2014). PLETHORA gradient formation mechanism separates auxin responses. Nature **515**:125–129.

Mason, M.G., Mathews, D.E., Argyros, D.A., Maxwell, B.B., Kieber, J.J., Alonso, J.M., Ecker, J.R., and Schaller, G.E. (2005). Multiple type-B response regulators mediate cytokinin signal transduction in *Arabidopsis*. Plant Cell **17**:3007–3018.

Matsuzaki, Y., Ogawa-Ohnishi, M., Mori, A., and Matsubayashi, Y. (2010). Secreted peptide signals required for maintenance of root stem cell niche in *Arabidopsis*. Science **329**:1065–1067.

Meyer, H.M., Teles, J., Formosa-Jordan, P., Refahi, Y., San-Bento, R., Ingram, G., Jonsson, H., Locke, J.C., and Roeder, A.H. (2017). Fluctuations of the transcription factor ATML1 generate the pattern of giant cells in the *Arabidopsis* sepal. Elife **6**. https://doi.org/10.7554/eLife.19131.

Miyashima, S., Koi, S., Hashimoto, T., and Nakajima, K. (2011). Non-cell-autonomous microRNA165 acts in a dose-dependent manner to regulate multiple differentiation status in the *Arabidopsis* root. Development **138**:2303–2313.

Miyashima, S., Roszak, P., Sevilem, I., Toyokura, K., Blob, B., Heo, J.O., Mellor, N., Help-Rinta-Rahko, H., Otero, S., Smet, W., et al. (2019). Mobile PEAR transcription factors integrate positional cues to prime cambial growth. Nature **565**:490–494.

Nawy, T., Lee, J.Y., Colinas, J., Wang, J.Y., Thongrod, S.C., Malamy, J.E., Birnbaum, K., and Benfey, P.N. (2005). Transcriptional profile of the *Arabidopsis* root quiescent center. Plant Cell **17**:1908–1925.

Normanly, J., Grisafi, P., Fink, G.R., and Bartel, B. (1997). *Arabidopsis* mutants resistant to the auxin effects of indole-3-acetonitrile are defective in the nitrilase encoded by the NIT1 gene. Plant Cell **9**:1781–1790.

Ohashi-Ito, K., and Bergmann, D.C. (2007). Regulation of the *Arabidopsis* root vascular initial population by LONESOME HIGHWAY. Development **134**:2959–2968.

Omelyanchuk, N.A., Kovrizhnykh, V.V., Oshchepkova, E.A., Pasternak, T., Palme, K., and Mironova, V.V. (2016). A detailed expression map of the PIN1 auxin transporter in *Arabidopsis thaliana* root. BMC Plant Biol. **16** (*Suppl 1*):5.

Patro, R., Duggal, G., Love, M.I., Irizarry, R.A., and Kingsford, C. (2017). Salmon provides fast and bias-aware quantification of transcript expression. Nat. Methods **14**:417–419.

Pena, M.J., Zhong, R., Zhou, G.K., Richardson, E.A., O'Neill, M.A., Darvill, A.G., York, W.S., and Ye, Z.H. (2007). *Arabidopsis* irregular xylem8 and irregular xylem9: implications for the complexity of glucuronoxylan biosynthesis. Plant Cell **19**:549–563.

Petricka, J.J., Winter, C.M., and Benfey, P.N. (2012). Control of *Arabidopsis* root development. Annu. Rev. Plant Biol. **63**:563–590.

Pi, L., Aichinger, E., van der Graaff, E., Llavata-Peris, C.I., Weijers, D., Hennig, L., Groot, E., and Laux, T. (2015). Organizer-derived WOX5 signal maintains root columella stem cells through chromatin-mediated repression of CDF4 expression. Dev. Cell **33**:576–588.

Pichon, X., Lagha, M., Mueller, F., and Bertrand, E. (2018). A growing toolbox to image gene expression in single cells: sensitive approaches for demanding challenges. Mol. Cell **71**:468–480.

Qiu, X., Mao, Q., Tang, Y., Wang, L., Chawla, R., Pliner, H.A., and Trapnell, C. (2017). Reversed graph embedding resolves complex single-cell trajectories. Nat. Methods **14**:979–982.

Rademacher, E.H., Moller, B., Lokerse, A.S., Llavata-Peris, C.I., van den Berg, W., and Weijers, D. (2011). A cellular expression map of the *Arabidopsis* AUXIN RESPONSE FACTOR gene family. Plant J. **68**:597–606.

Rhee, S.Y., Birnbaum, K.D., and Ehrhardt, D.W. (2019). Towards building a plant cell atlas. Trends Plant Sci. **24**:303–310.

Ryu, K.H., Huang, L., Kang, H.M., and Schiefelbein, J. (2019). Single-cell RNA sequencing resolves molecular relationships among individual plant cells. Plant Physiol. **179**:1444–1456.

Sabatini, S., Beis, D., Wolkenfelt, H., Murfett, J., Guilfoyle, T., Malamy, J., Benfey, P., Leyser, O., Bechtold, N., Weisbeek, P., et al. (1999). An auxin-dependent distal organizer of pattern and polarity in the *Arabidopsis* root. Cell **99**:463–472.

Sabatini, S., Heidstra, R., Wildwater, M., and Scheres, B. (2003). SCARECROW is involved in positioning the stem cell niche in the *Arabidopsis* root meristem. Genes Dev. **17**:354–358.

Santuari, L., Sanchez-Perez, G.F., Luijten, M., Rutjens, B., Terpstra, I., Berke, L., Gorte, M., Prasad, K., Bao, D., Timmermans-Hereijgers, J.L., et al. (2016). The PLETHORA gene regulatory network guides growth and cell differentiation in *Arabidopsis* roots. Plant Cell **28**:2937–2951.

Sarkar, A.K., Luijten, M., Miyashima, S., Lenhard, M., Hashimoto, T., Nakajima, K., Scheres, B., Heidstra, R., and Laux, T. (2007). Conserved factors regulate signalling in *Arabidopsis thaliana* shoot and root stem cell organizers. Nature **446**:811–814.

Satija, R., Farrell, J.A., Gennert, D., Schier, A.F., and Regev, A. (2015). Spatial reconstruction of single-cell gene expression data. Nat. Biotechnol. **33**:495–502.

Schlereth, A., Moller, B., Liu, W., Kientz, M., Flipse, J., Rademacher, E.H., Schmid, M., Jurgens, G., and Weijers, D. (2010). MONOPTEROS controls embryonic root initiation by regulating a mobile transcription factor. Nature **464**:913–916.

Shalek, A.K., Satija, R., Shuga, J., Trombetta, J.J., Gennert, D., Lu, D., Chen, P., Gertner, R.S., Gaublomme, J.T., Yosef, N., et al. (2014). Single-cell RNA-seq reveals dynamic paracrine control of cellular variation. Nature **510**:363–369.

Sharma, V.K., Carles, C., and Fletcher, J.C. (2003). Maintenance of stem cell populations in plants. Proc. Natl. Acad. Sci. U S A **100** (*Suppl 1*):11823–11829.

Smetana, O., Makila, R., Lyu, M., Amiryousefi, A., Sanchez Rodriguez, F., Wu, M.F., Sole-Gil, A., Leal Gavarron, M., Siligato, R., Miyashima, S., et al. (2019). High levels of auxin signalling define the stem-cell organizer of the vascular cambium. Nature **565**:485–489.

Staswick, P.E., Serban, B., Rowe, M., Tiryaki, I., Maldonado, M.T., Maldonado, M.C., and Suza, W. (2005). Characterization of an *Arabidopsis* enzyme family that conjugates amino acids to indole-3-acetic acid. Plant Cell **17**:616–627.

Swarup, K., Benkova, E., Swarup, R., Casimiro, I., Peret, B., Yang, Y., Parry, G., Nielsen, E., De Smet, I., Vanneste, S., et al. (2008). The auxin influx carrier LAX3 promotes lateral root emergence. Nat. Cell Biol. **10**:946–954.

Takano, M., Takahashi, H., Hirasawa, T., and Suge, H. (1995). Hydrotropism in roots: sensing of a gradient in water potential by the root cap. Planta **197**:410–413.

Trapnell, C., Cacchiarelli, D., Grimsby, J., Pokharel, P., Li, S., Morse, M., Lennon, N.J., Livak, K.J., Mikkelsen, T.S., and Rinn, J.L. (2014). The dynamics and regulators of cell fate decisions are revealed by pseudotemporal ordering of single cells. Nat. Biotechnol. **32**:381–386.

Treutlein, B., Brownfield, D.G., Wu, A.R., Neff, N.F., Mantalas, G.L., Espinoza, F.H., Desai, T.J., Krasnow, M.A., and Quake, S.R. (2014). Reconstructing lineage hierarchies of the distal lung epithelium using single-cell RNA-seq. Nature **509**:371–375.

Tusi, B.K., Wolock, S.L., Weinreb, C., Hwang, Y., Hidalgo, D., Zilionis, R., Waisman, A., Huh, J.R., Klein, A.M., and Socolovsky, M. (2018). Population snapshots predict early haematopoietic and erythroid hierarchies. Nature **555**:54–60.

van der Maaten, L., and Hinton, G. (2008). Visualizing Data using t-SNE. J. Mach. Learn. Res. **9**:2579–2605.

Wu, S., O'Lexy, R., Xu, M., Sang, Y., Chen, X., Yu, Q., and Gallagher, K.L. (2016). Symplastic signaling instructs cell division, cell expansion, and cell polarity in the ground tissue of *Arabidopsis thaliana* roots. Proc. Natl. Acad. Sci. U S A **113**:11621–11626.

Xie, Z., Lee, E., Lucas, J.R., Morohashi, K., Li, D., Murray, J.A., Sack, F.D., and Grotewold, E. (2010). Regulation of cell proliferation in the stomatal lineage by the *Arabidopsis* MYB FOUR LIPS via direct targeting of core cell cycle genes. Plant Cell **22**:2306–2321.

Yang, M., and Sack, F.D. (1995). The too many mouths and four lips mutations affect stomatal production in *Arabidopsis*. Plant Cell **7**:2227–2239.

Yu, G., Wang, L.G., Han, Y., and He, Q.Y. (2012). clusterProfiler: an R package for comparing biological themes among gene clusters. OMICS **16**:284–287.

Zhang, T.Q., Lian, H., Zhou, C.M., Xu, L., Jiao, Y., and Wang, J.W. (2017). A two-step model for de novo activation of WUSCHEL during plant shoot regeneration. Plant Cell **29**:1073–1087.

Zhong, S., Zhang, S., Fan, X., Wu, Q., Yan, L., Dong, J., Zhang, H., Li, L., Sun, L., Pan, N., et al. (2018). A single-cell RNA-seq survey of the developmental landscape of the human prefrontal cortex. Nature **555**:524–528.

Zurcher, E., Tavor-Deslex, D., Lituiev, D., Enkerli, K., Tarr, P.T., and Müller, B. (2013). A robust and sensitive synthetic sensor to monitor the transcriptional output of the cytokinin signaling network in planta. Plant Physiol. **161**:1066–1075.